Original Article

JCBFM

Journal of Cerebral Blood Flow & Metabolism
2018, Vol. 38(2) 317–332

DOI: 10.1177/0271678X17720816
journals.sagepub.com/home/jcbfm
SAGE

Occludin regulates glucose uptake and ATP production in pericytes by influencing AMP-activated protein kinase activity

Victor Castro, Marta Skowronska, Jorge Lombardi, Jane He, Neil Seth, Martina Velichkovska and Michal Toborek

Abstract

Energetic regulation at the blood-brain barrier is critical for maintaining its integrity, transport capabilities, and brain demands for glucose. However, the underlying mechanisms that regulate these processes are still poorly explored. We recently characterized the protein occludin as a NADH oxidase and demonstrated its influence on the expression and activation of the histone deacetylase SIRT-1. Because SIRT-1 works in concert with AMP-activated protein kinase (AMPK) (AMPK), we investigated the impact of occludin on this metabolic switch. Here we show that in blood-brain barrier pericytes, occludin promotes AMPK expression and activation, influencing the expression of glucose transporters GLUT-1 and GLUT-4, glucose uptake, and ATP content. Furthermore, occludin expression, AMP-dependent protein kinase activity, and glucose uptake were altered under inflammatory (TNFα) and infectious (HIV) conditions. We also show that pericytes share glucose and mitochondria with astrocytes, and that occludin levels modify the ability of pericytes to share those energetic resources. In addition, we demonstrate that murine mitochondria can be transferred from live brain microvessels to energetically impaired human astrocytes, promoting their survival. Our findings demonstrate that occludin plays an important role in blood-brain barrier pericyte metabolism by influencing AMPK protein kinase activity, glucose uptake, ATP production, and by regulating the ability of pericytes to interact metabolically with astrocytes.

Keywords

Blood-brain barrier, pericytes, occludin, glucose, AMP-activated protein kinase

Received 6 July 2016; Revised 15 May 2017; Accepted 12 June 2017

Introduction

The blood-brain barrier (BBB) is the regulated interface between the blood and the brain parenchyma and plays a paramount role in regulating brain homeostasis.[1] The ability of the BBB to cope with energetic demands during pathological conditions, like inflammation or infection, allows better physiological preservation of neurons under stress as they depend on the BBB for their nourishment and clearance of metabolic byproducts.[2] Specialization of the BBB on metabolic transport is critical to support neuronal function, most of the nutrient intake from the blood, and excretion of byproducts. These processes depend strongly on brain capillary endothelial cells that, by means of polarization, exhibit selective vectorial transport of ions and nutrients, including glucose.[3–5] Although endothelial cells constitute the anatomical/physiological basis of the barrier, they do not function alone. Astrocytes, pericytes, and the extracellular matrix complement endothelial cell function and regulate BBB physiology,[6,7] allowing the BBB to function as a dynamic unit capable of responding to a variety of neuronal metabolic demands.[7,8] Indeed, during increased neuronal activity, glucose uptake is enhanced in astrocytes,[9] and metabolic crosstalk was proposed to exist between astrocytes, pericytes and endothelial cells to regulate

Department of Biochemistry and Molecular Biology, Miller School of Medicine, University of Miami, Miami, FL, USA

Corresponding authors:
Michal Toborek, Department of Biochemistry and Molecular Biology, University of Miami School of Medicine, Miami 33136, FL, USA.
Email: mtoborek@med.miami.edu
Victor Castro, Department of Biochemistry and Molecular Biology, University of Miami School of Medicine, Miami 33136, FL, USA.
Email: victor.castro.villela@gmail.com

BBB functions.[10–15] Consequently, the capacity of astrocytes and pericytes to adapt to metabolic stress is crucial for the BBB to ensure that the delicate neuronal microenvironment is preserved and that an adequate flow of glucose into the brain is secured.

Endothelial cells and astrocytes have been thoroughly studied throughout the literature;[16] however, BBB pericyte physiology remains largely undescribed. Indeed, pericytes have been the most overlooked cells of the BBB[17] due to the absence of specific cell markers and the cell-subpopulation heterogeneity that complicate their isolation and in-vivo identification. Pericytes are essential for maintaining microvascular viability, provide structural support to endothelial cells, and confer vasodynamic capabilities to capillaries. Angiogenesis, maturation of the BBB, and maintenance of its functions appear to rely on pericytes, which also contribute to endothelial cell longevity by preventing apoptosis.[18,19] Despite this progress in understanding pericyte functions, their molecular physiology and intercellular communication mechanisms are still poorly understood. In the BBB, pericytes are in direct contact with endothelial cells and cover approximately 30% of their abluminal surface.[19] They also express molecules that were originally thought to be exclusive to endothelial cells, namely, tight junction protein, such as claudin-12, ZO-1, and occludin,[20] which suggests functions for these proteins beyond the originally described regulation of BBB barrier integrity.

Recent evidence indicates that occludin is expressed in a variety of cells that undergo substantial metabolic alterations under stress, such as epithelial/endothelial cells,[21] pericytes,[20] neurons,[22] astrocytes,[21,22] oligodendrocytes,[23] dendritic cells,[24] monocytes/macrophages,[25] lymphocytes,[26] and myocardium.[27] The precise molecular function of occludin remained ambiguous since its discovery; however, we recently characterized occludin as a NADH oxidase that, in pericytes, influences expression and activation of the NAD^+-dependent histone deacetylase SIRT-1.[25] The metabolic significance of this novel function was exemplified under the setting of HIV infection, where occludin was shown to regulate expression and activation of SIRT-1, influencing HIV transcription. SIRT-1 plays a key role regulating energy metabolism by interacting with the metabolic regulator AMP-activated protein kinase (AMPK) to control metabolic adaptation to stress.[28] AMPK also plays a prominent regulatory role in glucose uptake,[29] as it regulates expression and cell surface translocation of glucose transporters.[30] Thus, expression and activation of AMPK/SIRT-1 constitute a signaling hub that regulates gene expression and directs energy metabolism under physiological and pathological conditions.[31] Because NAD^+ is a strong activator of AMPK,[32] we hypothesized that occludin can regulate cell energetics and metabolism by influencing SIRT-1/AMPK activity.

Materials and methods

Cell culture

Primary human brain capillary pericytes and astrocytes (ScienCell, Carlsbad, CA, USA) were cultured in 5% CO_2 at 37°C in pericyte or astrocyte growth medium (ScienCell), following standard cell culture procedures, and used between passages 2 and 7. Human cerebral microvascular endothelial cells (HCMEC-D3 cells) were cultured as previously described.[33] Human fibroblasts (CCD-1099Sk) were obtained from the American Type Culture Collection (ATCC, Manassas, VA, USA) and cultured according to ATCC guidelines. For confocal microscopy imaging, cells were cultured directly on six-well plates and visualized with water-immersion lenses. In-cell ELISA and spectrofluorometry were performed in cells seeded on 96-well opaque, polystyrene plates (Nunclon Delta Surface, Thermo Scientific-Nunc, Denmark) without additional coating. Pericytes were molecularly characterized as previously shown.[25] In the selected experiments, cells were treated with recombinant human TNFα (250 ng/mL; Thermo Fisher Scientific, USA) for 2 h, 5-Aminoimidazole-4-carboxamide ribonucleotide (AICAR, AMPK activator, 1 mM; Sigma Aldrich, USA) or dorsomorphin (AMPK inhibitor, 40 μM; Sigma Aldrich, USA) for 12 h. HIV infection was performed by adding cell-free HIV1-NL43 to the culture media as previously shown[25] (300,000 cpm per 50 μL of growth media covering ~25,000 cells).

Quantitation of glucose uptake

Cells were grown to 75% confluency on 96-well plates. The glucose analogue 2-N-7-nitrobenz-2-oxa-1,3-diazol-4-yl-amino-2-deoxyglucose (2-NBDG) (0.15 mg/mL; Life Technologies, USA) and the nucleic acid stain DRAQ-5 (1:200; Abcam, USA) were simultaneously added to the growth medium and incubated for 10 min at 37°C. Excess of 2-NBDG and DRAQ-5 was removed by rinsing with PBS. Plates were sealed with optical film (Microamp; Applied Biosystems, USA) and 2-NBDG fluorescence intensity was read with a Gemini EM spectrofluorometer (Molecular Devices, Sunnyvale, CA, USA) using the following parameters: top-read, 6-flashes, normal speed, temperature 24–26°C, 460 nm – cutoff 475 nm, spectral detection

500–580 nm. Quantitation was performed by calculating the area under the curve for the recorded spectral range. Data were normalized to the change in DRAQ-5 fluorescence intensity in all samples for every experiment.

Spectrally resolved in-cell ELISA and immunoblotting

Immunoblotting and spectrally resolved in-cell ELISA (SPRICE) were performed as previously described.[25] For SPRICE, cells were cultured in 96-well plates, stained with DRAQ-5 (1:100, Cell Signaling Technology, USA) as recommended by the manufacturer, and fixed with ice-cold methanol. Non-specific binding sites were blocked with BlockAid (Invitrogen, Carlsbad, CA, USA) for 2 h at room temperature (22°C). Cells were then immunolabeled with antibodies validated for in-cell ELISA or cell-cytometry and directed against GLUT-1, GLUT-4, occludin, NFκB p65, acetyl (K310)-NFκB, total AMPK, phospho (T172)-AMPK, total SP1, and phospho (T453)-SP1 (all antibodies from Abcam, USA), mixed with fluorescently labeled secondary antibodies (Alexa Fluor 405, 488, 594, or Dylight 680), and incubated for 3 h at room temperature (22°C).

Multiwell plates were sealed with optical film (Microamp, Applied Biosystems, USA) and read in a Gemini-EM spectrofluorometer (Molecular Devices, USA) using 6-flashes at 24–26°C. Fluorophore excitation wavelengths (Ex), excitation cutoff (C), and recorded emission spectral ranges (Em) were as follows (values shown in nm): DRAQ-5: Ex600, C610, Em 650-780; Dylight 680: Ex650, C665, Em680-800; Alexa 594: Ex545, C570, Em590-650; Alexa 405: Ex380, C420, Em424-450; Alexa 488: Ex480, C495, Em505-600; and Alexa 594: Ex545, C570, Em590-650. Spectra fell within the linear detection range without overlapping or channel cross-bleeding, enabling simultaneous quantification of expression/activation of several molecules in the same cell. Acquired spectra were visualized in Soft-Max Pro (v 6.1 Molecular Devices, USA) and exported to Microsoft-Excel datasheets. The area under the curve (spectral intensity) was calculated for each recorded spectrum in the following ranges: DRAQ-5, 675–685 nm; Alexa 405, 424–450 nm; Alexa 488, 505–600 nm; Alexa 594, 590–650 nm; and Dylight 680, 695–725 nm. Expression levels were normalized to the difference in DRAQ-5 intensity (cell density) across the measured samples in each experiment.

Levels of active AMPK, NFκB and SP1 were expressed as the ratio between their active and total forms to eliminate bias caused by changes in total expression. All reported measurements were within linear detection range of the equipment.

Occludin and ZO-1 depletion. Occludin overexpression

Cells were grown to 75% confluency in 96-well plates. For occludin silencing, medium was exchanged for Opti-Mem (Invitrogen, USA) and cells were transfected with Lipofectamine 2000 (Invitrogen), following manufacturer's instructions, with 6.25 pM per well of anti occludin 27-mer human siRNA (Trilencer-27 duplex-siRNA SR303274A: UGCACCAAGCAAU GACAUAUAUGGT, OriGene), diluted in RNA resuspension buffer (100 mM KAc, 30 mM HEPES, pH 7.0). ZO-1 was silenced with three unique 27mer siRNA duplexes (TJP1 Trilencer-27 Human siRNA, Origene) SR322042A, GCUAUUGAAUGUCCCU GAUCUUUCT; SR322042B, GAAGAUAUUGUUC GGUCCAAUCATT; SR322042C, CUAGAUACUG UAUCAUGACAAAGAC using similar transfection procedure. Control siRNA (Trilencer-27 Universal scrambled negative control siRNA duplex SR30004; OriGene) or custom made control (AAAGAG CGACUUUACACACdTdT; Dharmacon, Thermo Scientific) were similarly transfected. Cells were incubated with the transfection reaction for up to 24 h without observing morphological anomalies or unusual cell detachment. Occludin overexpression was achieved by removing siRNA-containing medium at 12 h post-silencing and substituting it with fresh siRNA-free growth medium for a period of 48 h as previously shown.[25] This procedure results in a reactive increase in occludin levels by ~20% over WT cells. Occludin levels were monitored and quantified by SPRICE.[25]

ATP determination

Cells were grown to 75% confluency in 12-well plates. Growth medium was washed off with PBS and cells were flash frozen in liquid nitrogen. An ATP determination kit (ThermoFisher USA) was then used following manufacturer's instructions. Briefly, 10 µL of each sample was incubated in a reaction buffer containing DTT, d-luciferin, and firefly luciferase. Production of oxyluciferin was measured by luminescence intensity reading at 560 nm.

Live cell imaging of glucose and mitochondria transfer

Pericytes were cultured until 75–80% confluency and incubated for 10 min with 0.5 µM tetramethylrhodamine-ethyl-ester (TMRE ThermoFisher, USA) and 0.15 mg/mL 2-NBDG diluted in growth medium. Simultaneously, a similarly confluent culture of astrocytes, endothelial cells or fibroblasts was incubated for

10 min with the intracellular cell mask bromomethyl-tetrahydro-pyrano-quinolin (Violet BMQC Life Technologies, USA). Cells were washed thoroughly with PBS, trypsinized 10 min later and co-cultured in 12-well plates with DMEM-based growth medium. They were transferred to an upright confocal microscope (Olympus Fluoview2000) 30 min after plating. 2-NBDG, TMRE and BMQC fluorescence were recorded simultaneously with a bright field image reference. Extracellular transfer of TMRE/2-NBDG, or direct astrocyte staining with TMRE/2-NBDG that could have remained in the pericyte medium after washing, was ruled out by incubating astrocytes with the medium in which the pericytes were incubated before trypsinization followed by negative detection of TMRE and 2-NBDG staining under confocal microscopy.

Isolation of murine live brain microvessels and incubation with human astrocytes

Animal procedures were approved by the University of Miami Institutional Animal Care and Use Committee following National Institutes of Health (NIH) guidelines, conducted in accordance with the relevant regulations, and in compliance with Animal Research: Reporting in Vivo Experiments (ARRIVE) guidelines. Three-month-old, C57BL/6 male mice were sacrificed and microvessel isolation was performed as previously described.[34] Briefly, their brains were immediately removed and immersed in ice-cold preservation solution (Hydroxyethyl starch–pentafraction 50 g/L, lactobionic acid 35.83 g/L, magnesium sulfate heptahydrate 17.83 g/L, raffinose pentahydrate 17.83 g/L, potassium hydroxide 5.61 g/L, potassium dihydrogen phosphate 3.4 g/L, allopurinol 0.136 g/L, adenosine 1.34 g/L, and glutathione 0.922 g/L). They were next minced with a scalpel until obtaining $\sim$2 mm^3 fragments, passed five times through a 26G needle, and centrifuged at 10,000$\times g$ for 15 min at 4°C in dextran 70 (final concentration 15% in preservation solution). The microvessel-containing pellet was resuspended and incubated in preservation solution containing TMRE (0.5 µM) and 2-NBDG (0.15 mg/mL) for 10 min at 37°C. The microvessels were next passed through a 70 µM strainer, extensively washed five times with warm preservation solution, and recovered by back-flushing the strainer into a petri dish. Microvessels were then added to the growth medium in which human primary astrocytes were cultured to 90% confluency (35 mm petri dishes). Each dish received all isolated microvessels from a whole brain.

Immunofluorescence

Pericytes were cultured in translucent 12-well plates, fixed with ice-cold methanol for 30 min, blocked with Block-AID (Invitrogen, USA) for 45 min at room temperature, and incubated with a cocktail containing primary anti-GLUT-1, GLUT-4, and occludin antibodies (1:300) pre-mixed with fluorescently labeled secondary antibodies for 2 h at room temperature. Anti-LAMP1 antibody (1:300) was obtained from Abcam (USA). After washing, 3 ml of PBS was added to each well and the samples were recorded using laser scanning confocal microscopy and water-dipping lenses.

Image analysis

Confocal microscopy images were recorded using Olympus proprietary software (FLUO-VIEW), saved as meta-data enriched TIFF files, and analyzed with Image-J (NIH, USA).

Statistical analysis

Datasets were organized in Excel 2013 (Microsoft) and exported to Prism v.6 (GraphPad software). Data were tested for normality by D'Agostino-Pearson and Shapiro-Wilk tests with confidence interval of 99%. For univariate datasets, one-way ANOVA or Kruskal–Wallis test, if non parametric, was performed to determine the p values. $P < 0.05$ was considered statistically significant. Groups to be compared were selected during experimental design and analyzed with Fisher's Least Square Difference post hoc test. Multivariate datasets were analyzed with two-way ANOVA. Binary datasets were compared using Welch-corrected t-tests, or Mann–Whitney tests if non-parametric.

Results

Occludin levels influence glucose uptake in BBB pericytes

We first determined the basal rate of glucose uptake in human primary pericytes and compared this activity to that of other BBB cell types: primary astrocytes and endothelial cells. Using the fluorescent glucose analog 2-NBDG, we observed that pericyte glucose intake is comparable to that of astrocytes but several times higher than in endothelial cells (Figure 1(a)). Using spectrally resolved in-cell ELISA (SPRICE), we similarly determined that expression of GLUT-1 and GLUT-4 transporters is comparable between pericytes and astrocytes. Although endothelial cells express similar levels of GLUT-1, their expression of GLUT-4 is remarkably lower than astrocytes and pericytes (Figure 1(b) and (c)). These observations suggest that pericytes may share basal metabolic characteristics with astrocytes, but not with endothelial cells. In line with

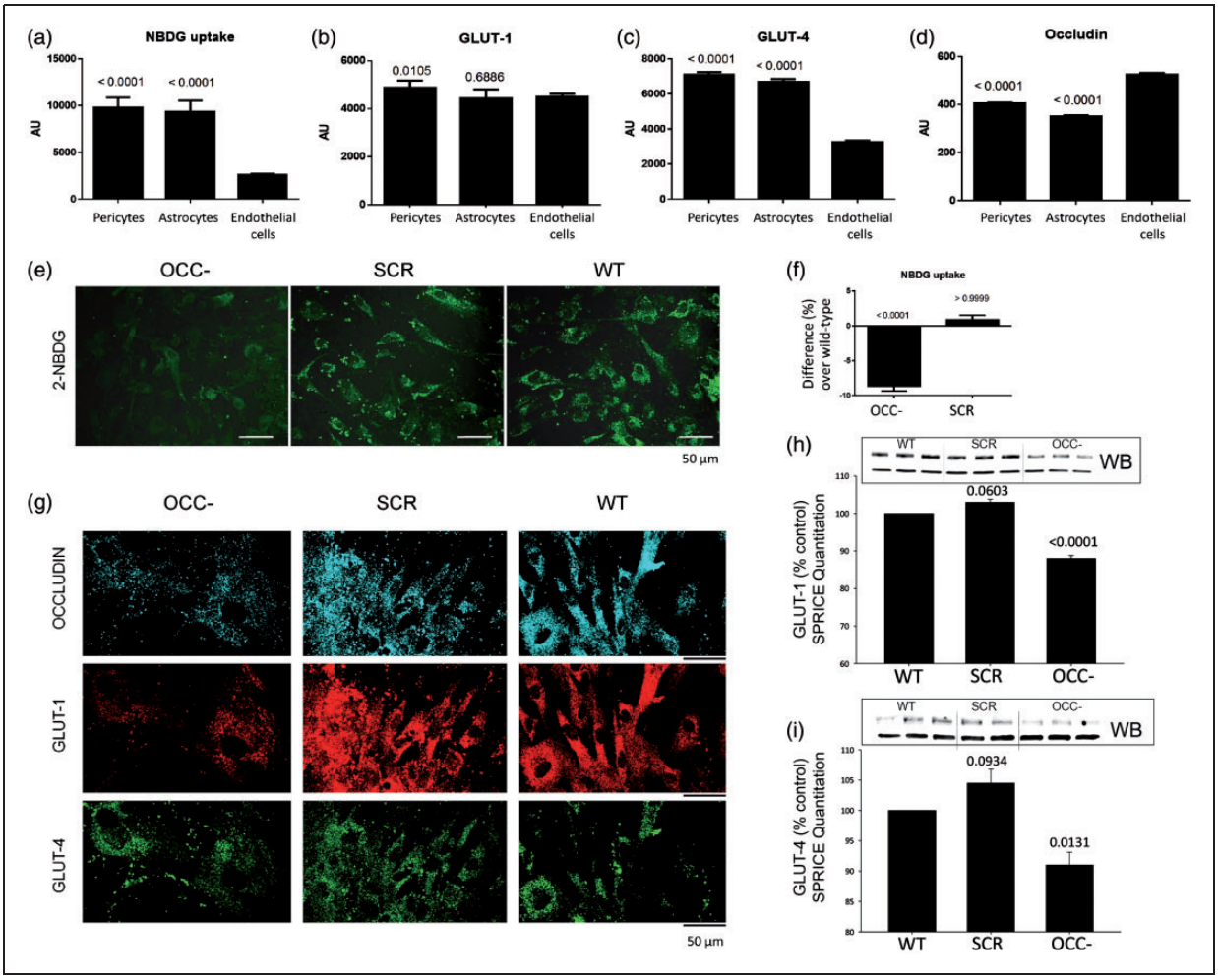

Figure 1. Glucose uptake and expression of GLUT-1 and GLUT-4 in pericytes is mediated by occludin. (a) Cellular uptake of the fluorescent glucose analog 2-NBDG (0.15 mg/mL, 10 min) as measured fluorospectrometrically. (b) Spectrally resolved in-cell ELISA (SPRICE) quantitation of GLUT-1, (c) GLUT-4 and (d) occludin in the same cells shown in (a). Average ± SEM, $n = 6$. (e) Representative confocal microscopy images of live pericytes after being incubated for 10 min with 2-NBDG. Pericytes were previously treated with anti-occludin siRNA (OCC−), negative-control siRNA (SCR), or were not treated (wild-type, WT). (f) Fluorospectrometrical quantitation of 2-NBDG from experiments illustrated in (e). (g) Confocal microscopy imaging of pericytes treated as in (e), showing expression of occludin, GLUT-1, and GLUT-4. These cells were then treated for SPRICE to quantify (h) GLUT-1 and (i) GLUT-4. Representative western blots (WB) are shown to illustrate GLUT-1 and GLUT-4 protein expression in WT and OCC− pericytes. (f, h, i) Graphs represent the average percentual difference over WT values (horizontal axis at 0), SEM, $n = 6$, p vs. WT. All measurements were normalized against their corresponding DRAQ-5 intensities.

our hypothesis that occludin can regulate cell metabolism, we measured expression of occludin in all three cell types. Occludin levels in pericytes are equivalent to those in astrocytes but lower than in endothelial cells (Figure 1(d)).

The influence of occludin on pericyte glucose uptake and glucose transporter expression was explored in pericytes by anti-occludin siRNA treatment (12 h) before glucose uptake was measured. Confocal microscopy imaging of live pericytes showed reduced intracellular 2-NBDG fluorescence in occludin deficient cells as compared to negative-control siRNA-treated or non-treated cells (Figure 1(e)). These changes were further quantified by fluorospectrometry (Figure 1(f)). Furthermore, confocal microscopy, western blot, and SPRICE quantitation showed that the expression of GLUT-1 and GLUT-4 was lower in occludin-deficient cells than in their negative-control siRNA-treated counterparts (Figure 1(g) to (i)). Treatment of pericytes with siRNA against ZO-1, an occludin functional partner, did not induce changes in GLUT-1 or GLUT-4 protein levels (Supplemental Figure 1), indicating that the observed changes were occludin-specific.

Occludin expression regulates AMPK phosphorylation and correlates with cellular ATP content

Our results indicated that occludin is involved in controlling expression of glucose transporters and glucose uptake, known to be regulated by AMPK. Occludin is a NADH oxidase that activates the NAD+-dependent histone deacetylase SIRT-1,[25] and could also induce the activation of other NAD^+-sensitive molecules like AMPK.[32] Therefore, we evaluated whether AMPK activation correlated with occludin expression: the expression ratio of phosphorylated-(*T-172*) vs. total-AMPK was strongly reduced (Figure 2(a)), while total AMPK expression was doubled in occludin deficient pericytes (OCC-) (Supplemental Figure S2A). Overexpression of occludin induced a subtle and consistent increase in phosphorylated and total AMPK (OCC+; Figure 2(a) and Supplemental Figure S2A, respectively).

AMPK is a critical cell-energetics regulator; therefore, we quantified the content of ATP in pericytes, and measured how it changed upon pharmacological AMPK super-activation by AICAR, or inhibition by dorsomorphin (compound C). In wild-type cells, AMPK super-activation elevated ATP content by 50% when compared to control values; however, dorsomorphin did not affect ATP levels (Figure 2(b), AMPK+ and AMPK−, respectively). We next measured ATP content in pericytes treated with anti-occludin siRNA. Occludin deficiency (OCC−) resulted in decreased ATP levels (Figure 2(c), NT), and AMPK

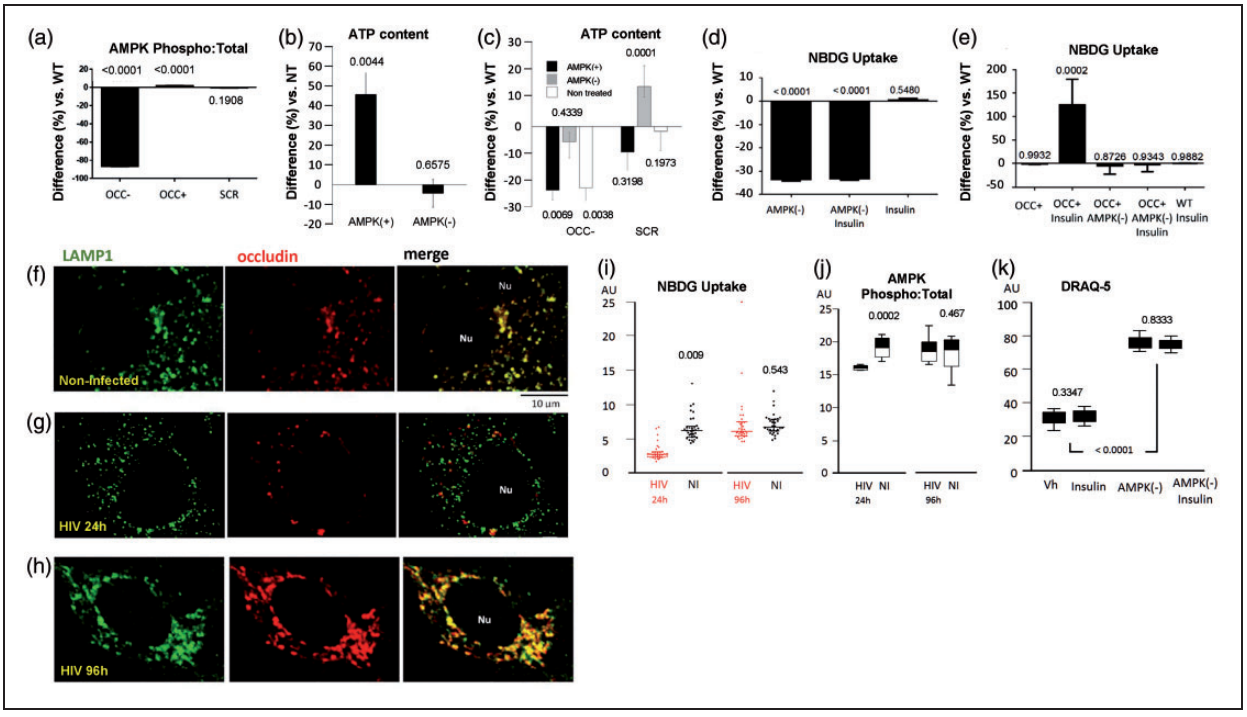

Figure 2. Occludin influences energetic processes by controlling AMPK activation. (a) SPRICE quantitation of active (phospho) AMPK in occludin-deficient (OCC−), occludin overexpressing (OCC+), and control (SCR) pericytes. Values represent the ratio of phosphorylated vs. the respective total AMPK expression, normalized against DRAQ-5. (b) ATP content in pericytes treated with AICAR (AMPK activator, AMPK+) or dorsomorphin (AMPK inhibitor, AMPK−). (c) ATP quantitation in occludin-deficient (OCC−) or control (SCR) pericytes treated or not with AICAR or dorsomorphin as in (c). (d) Fluorospectrometric quantitation of 2-NBDG taken up by WT-pericytes treated with dorsomorphin (AMPK-) and/or insulin. (e) Similar 2-NBDG quantitation in occludin overexpressing (OCC+) pericytes treated with dorsomorphin and/or insulin. Graphs show average percentual difference over WT pericytes treated with PBS (Vh), represented by the horizontal axis at 0, SEM, n=6, p vs. WT. (f) Representative confocal microscopy images of WT pericytes immunostained for the lysosomal marker LAMP1 (green) and occludin (red). Nu: Cell nucleus. (g) Representative confocal microscopy images of HIV-infected pericytes 24 h post-infection (occludin depletion phase), immunostained as in (f). (h) Representative confocal microscopy images of HIV-infected pericytes 96 h post-infection (occludin recovery phase) and immunostained as in (f) and (g). Non-infected (NI) and HIV-infected pericytes at different time points post infection were analyzed by SPRICE to quantify (i) 2-NBDG uptake and (j) active AMPK (graph shows the ratio between phosphorylated and total AMPK levels). (k) Fluorospectrometric quantitation of stoichiometric DRAQ-5 uptake as an index of cell proliferation in non-infected pericytes treated with vehicle (Vh), insulin, and dorsomorphin (AMPK-). (i to k), average ± SEM, $n = 6$, p vs. WT.

stimulation with AICAR was unable to restore this effect (Figure 2(c), AMPK+). These observations suggest that occludin and AMPK form a partnership crucial for cellular energetics. The inability of AICAR to restore ATP levels in occludin deficient cells suggests that occludin is a powerful AMPK regulator.

We further explored the role of AMPK/occludin interactions on pericyte metabolism by evaluating the impact of insulin on glucose uptake and GLUT-1 and GLUT-4 expression. Glucose uptake in pericytes was unaltered upon insulin treatment; however, inhibition of AMPK by dorsomorphin markedly decreased glucose uptake (Figure 2(d), AMPK−). Occludin overexpression or insulin alone was unable to modify glucose uptake (Figure 2(e)). Nevertheless, the combination of these factors strongly increased glucose uptake (Figure 2(e), OCC+ Insulin), in a manner that was entirely abolished when AMPK activity was inhibited (Figure 2(e), AMPK−).

Expression of GLUT-1 and GLUT-4 was decreased when AMPK was inhibited, but not upon insulin treatment, in wild type pericytes (Supplemental Figures S2B and S2C). Occludin overexpression enhanced the expression of both transporters in an AMPK-mediated manner. Interestingly, the combination of insulin and occludin overexpression resulted in elevation of GLUT-4, but not GLUT-1, expression levels. Similar to the ability of insulin to enhance glucose uptake in occludin overexpression conditions, the observed elevation of GLUT-4 was reverted if AMPK activity was inhibited (Supplemental Figures S2D and S2E).

Occludin confers insulin sensitivity to pericytes and regulates AMPK activity

Up to this point, our data show that although AMPK requires occludin to respond to stimulation by AICAR and induce ATP production, occludin also depends on AMPK to exert influence on glucose uptake and expression of glucose transporters. Previous work has shown that AMPK docks to the lysosomal membrane to be activated by LKB1 (Liver Kinase B1; also known as Serine/Threonine Kinase 11, STK11).[35] Interestingly, confocal microscopy indicated that, in pericytes, occludin colocalizes with lysosome membranes as determined by immunostaining with lysosomal-associated membrane protein 1 (LAMP-1) (Figure 2(f)).

We recently showed that infection of pericytes with HIV causes initial occludin depletion but pericytes recover occludin levels within 96 h.[25] We used this model to evaluate whether pathological alterations of occludin levels could influence AMPK activity and its lysosomal localization. Analysis of HIV-infected pericytes showed decreased lysosomal localization of occludin 24 h post infection (Figure 2(g)); however, this localization was then increased during the occludin recovery phase (Figure 2(h)). Glucose uptake and AMPK activation were correlated with occludin levels. They were decreased in HIV-infected cells 24 h post infection, when occludin levels were diminished, and recovered 96 h post infection during occludin restoration phase (Figure 2(i) and (j), respectively).

The occludin-depletion phase also induced pericyte proliferation in HIV-infected pericytes (Supplemental Figure S3A). Treatment of non-infected pericytes with dorsomorphin resulted in enhanced proliferation (Figure 2(k)), suggesting that occludin levels and AMPK activity may control the ability of pericytes to proliferate. In a similar manner, treatment of pericytes with TNFα (250 ng/mL for 2 h) decreased occludin levels, diminished glucose uptake, and enhanced their proliferation (Supplemental Figures S3B–S3D, respectively). The involvement of occludin in pericyte proliferation was further explored by quantifying DRAQ-5 uptake. As indicated in Supplemental Fig S3E, pericytes proliferated more than their wild-type and negative-control siRNA-treated counterparts, 12 h after incubation with anti-occludin siRNA.

Occludin influences NFκB and SP1 activation and chromatin organization

NFκB contributes to integration of the cellular responses during inflammation. In addition, transcriptional regulation of GLUT-1 and GLUT-4 is mediated by the transcription factors NFκB and SP1. Therefore, we investigated the influence of occludin on activation of NFκB and SP1 in pericytes. Occludin depletion resulted in a slight but consistent elevation of acetylated (active) NFκB p65, accompanied by strong reduction of total p65 levels. Occludin overexpression, however, caused the opposite effect: a strong decrease in active p65 and a slight increase in its total levels (Figure 3(a) and (b)). Similarly, occludin overexpression reduced SP1 phosphorylation (active form), which correlated with a strong elevation in total SP1 levels. However, occludin depletion did not alter SP1 phosphorylation and/or its total levels (Figure 3(c) and (d)). The influence of occludin on the expression and activity of these transcription factors, AMPK and glucose transporters, together with our previous findings showing correlation between occludin and the activity of the histone deacetylase SIRT-1, prompted the possibility that nuclear reorganization may occur in response to variations in cellular occludin content. Therefore, we evaluated the spatial organization of the nucleosomal histone H2.A and the linker H1. Occludin depletion correlated with enhanced colocalization of both histones (Figure 3(e) and (f)), suggesting that chromatin is more densely packed in the absence of occludin than it is in wild-type cells.

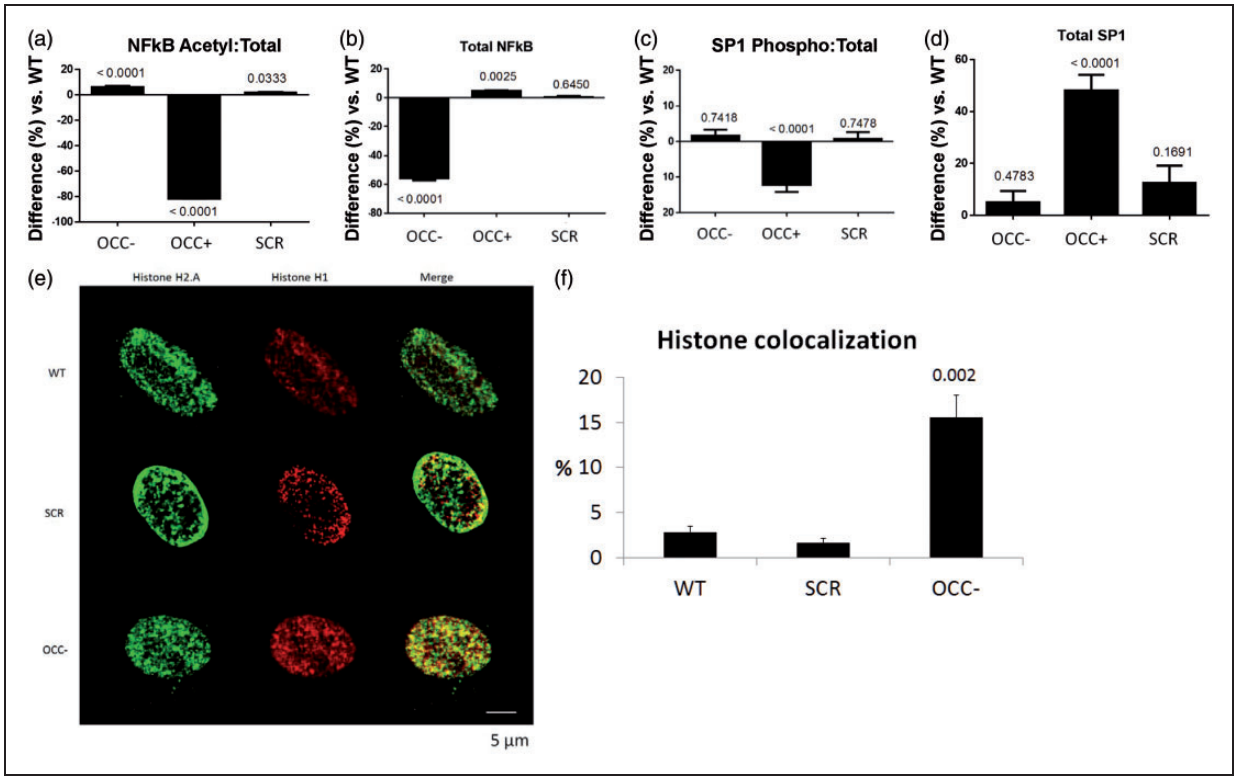

Figure 3. Occludin impacts activation of NFκB and SP1, and causes chromatin relaxation. (a) SPRICE quantitation of acetyl-NFκB in occludin-deficient (OCC−), occludin overexpressing (OCC+) and control (SCR) pericytes. The values represent a ratio between acetylated and their respective (b) total NFκB levels. (c) Similar quantitation of phosphorylated and (d) total SP1 in the same cells shown in (a) and (b). Graphs show average percentual difference over WT pericytes (horizontal axis at 0), SEM, $n=6$, p vs. WT. (e) Representative confocal microscopy images of pericyte nuclei stained with antibodies against the nucleosomal histone H2.A (green) and the linker histone H1 (red) in WT, SCR and OCC− pericytes. (f) The average percentage of histone h2.A signal from E that colocalized with histone H1. Average ± SEM; 10 fields from three separate experiments.

Pericytes share glucose and mitochondria with astrocytes in an occludin-modulated manner

Altogether, our findings indicated that occludin can influence crucial aspects of pericyte energetics and metabolism. However, we sought to further explore if occludin also influences the manner in which pericytes interact metabolically with other cells in the BBB, particularly with astrocytes, and evaluated the capacity of pericytes to share glucose with them. Pericytes were allowed to take up 2-NBDG before being mixed with cell tracker-labeled (Violet BMQC) astrocytes in co-culture. Using confocal microscopy, we observed that most of the 2-NBDG was promptly (within 30 min) transferred from pericytes to astrocytes (Figure 4(a)), and after 24 h the entire 2-NBDG load had been transferred from pericytes to astrocytes (Figure 4(b)), evidencing that pericytes can readily transfer glucose to astrocytes.

Interestingly, when pericytes were treated with anti-occludin siRNA, transfer of 2-NBDG to astrocytes was increased during the first 30 min, and at 24 h all 2-NBDG signal was now present in astrocytes, albeit with a total lower intensity than the astrocytes that received 2-NBDG from wild-type pericytes (Figure 4(c) to (f)). This less intense 2-NBDG signal correlates with the lower capacity of occludin-depleted pericytes to take up glucose (shown in Figure 1(e)). It is noticeable that once astrocytes received the glucose analogue, regardless of the source (WT or OCC- pericytes), they distributed it throughout the whole astrocytic network without delivering it back to pericytes [note cyan signal in most astrocytes (deep blue), combined with the absence of green signal in pericytes (thin arrows) in Figure 4(b), (d) and (f)]. Quantitative data are shown in Figure 4(g) and (h).

Similar experiments showed glucose transfer also occurred between pericytes and brain capillary endothelial cells or BBB-unrelated cells such as fibroblasts (Supplemental Figure S4). Similar to pericyte-astrocyte co-cultures, occludin depletion in pericytes increased glucose transfer from pericytes to fibroblasts (Figure S4B). On the other hand, glucose transfer from pericytes to endothelial cells was decreased upon

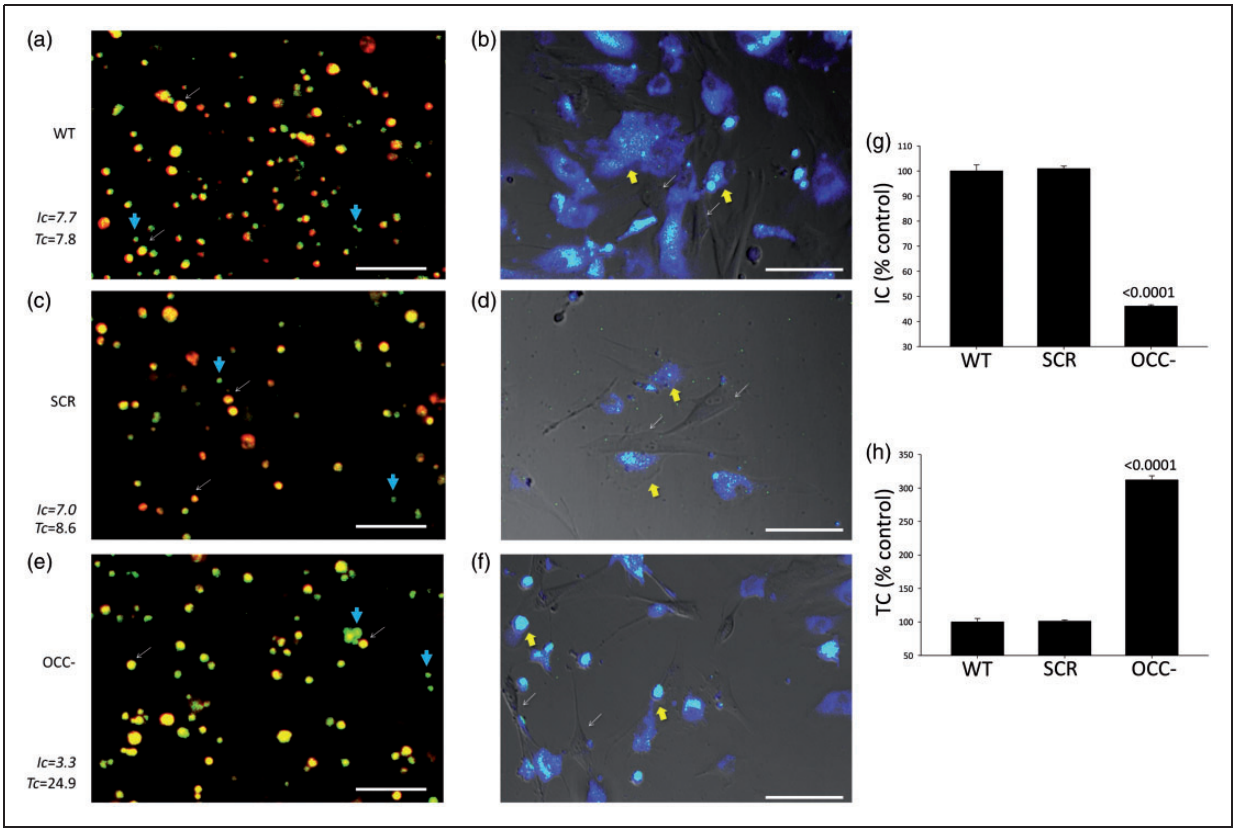

Figure 4. Pericytes share glucose with astrocytes in an occludin-modulated manner. (a) Confocal microscopy of a representative live pericyte-astrocyte co-culture 30 min after plating. Pericytes were pre-loaded with 2-NBDG (green; e.g. blue thick arrows) and astrocytes with violet-BMQC (cell mask, red) but not with 2-NBDG. Colocalization of both signals (yellow-orange; e.g. white thin arrows) indicated that astrocytes had received 2-NBDG. Intensity coefficient (Ic) represents the whole 2-NBDG fluorescence intensity normalized to the surface it occupies, regardless of cell type. A larger Ic means more 2-NBDG was introduced into the system (taken up by pericytes). Transfer coefficient (Tc) represents the fraction of astrocytic surface occupied by 2-NBDG normalized against the Intensity coefficient. A larger Tc implicates more 2-NBDG was distributed across all possible astrocytes, and represents greater transferred volumes. Data correspond to the quantitation of the images shown. They are representative of three separate experiments. (b) Distribution of 2-NBDG in the same co-culture shown in (a), 24 h after plating. Pericytes are devoid of any stain (e.g. white thin arrows). 2-NBDG signal (green) colocalizing with astrocytes is seen as cyan/white (e.g. yellow thick arrows). (c) Similar co-culture as in (a) recorded 30 min post-plating; however, pericytes were treated with negative-control siRNA (SCR) before being loaded with 2-NBDG. (d) Distribution of 2-NBDG (green/cyan) in the same co-culture shown in (c), 24 h post-plating. (e) Similar co-culture as in (a) and (c), recorded 30 min post-plating; however, pericytes were treated with anti-occludin siRNA (OCC−) before being loaded with 2-NBDG. (f) Distribution of 2-NBDG (green/cyan) in the same co-culture shown in (e), 24 h post-plating. All images are representative of three separate experiments. (g) Average intensity (Ic) and H) Transfer (Tc) coefficients depicting transcellular glucose transport between pericytes and astrocytes as shown in (a) to (c). $n = 3$, p vs. WT.

occludin depletion (Figure S4A). These results indicate highly specific regulation of intercellular glucose sharing between cells of neurovascular unit.

In parallel experiments, pericytes were allowed to take up 2-NBDG, while a second set of pericytes was labeled with TMRE, which is captured and trapped only in active mitochondria, before co-culturing. Following a 12-h incubation, we observed that some of the TMRE-labeled mitochondria migrated into 2-NBDG containing pericytes, while some 2-NBDG was also shared with TMRE labeled pericytes (Figure 5(a)). Further experiments showed that most mitochondria were transferred 24 h after pericytes were seeded (Figure 5(b)). This was accompanied by numerous mitochondria embedded into cell-interconnecting filopodia (Figure 5(c), arrows) and mitochondrial aggregation at cell–cell contacts (Figure 5(d) to (f)).

These findings suggest that pericytes have the capacity to transfer vital resources to other cells; therefore, we investigated next whether they could also transfer mitochondria to astrocytes. Live cell imaging of cell-tracker-labeled astrocytes co-cultured with TMRE-labeled pericytes revealed that astrocytes

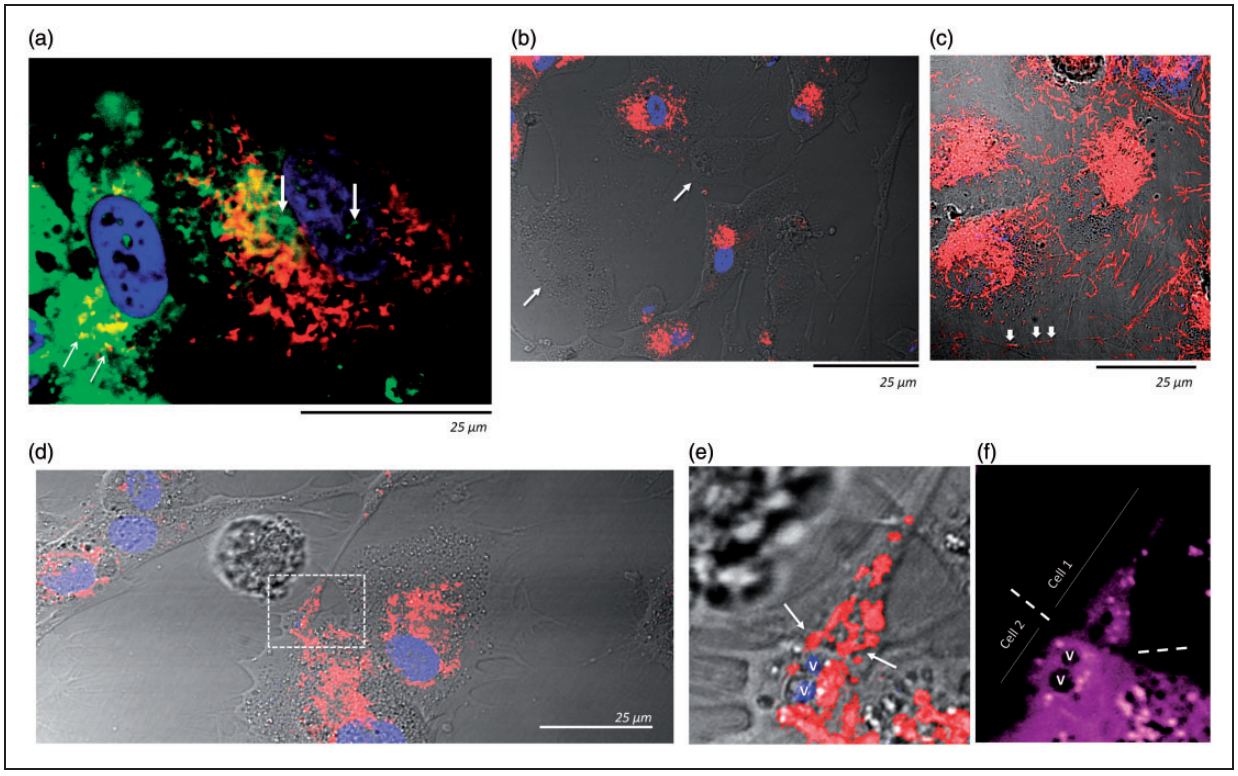

Figure 5. Pericytes share glucose and mitochondria between themselves. (a) Confocal microscopy imaging of two living pericytes, 12 h after plating. One was pre-loaded with 2-NBDG (green) while the other was stained with TMRE (live mitochondria) but not 2-NBDG. 2-NBDG can be seen in the cytosol and nucleus (e.g. thick vertical arrows) of the TMRE labeled pericyte, while TMRE-stained mitochondria can be seen (e.g. yellow colocalization, thin diagonal arrows) in the cytosol of the pericyte that was only loaded with 2-NBDG. (b) Representative confocal microscopy image of a live co-culture of two sets of pericytes; one of them was pre-stained only with TMRE and the other only with the nuclear dye DRAQ-5, 24 h post plating. Most of the TMRE-labeled mitochondria have been transferred to DRAQ-5 stained pericytes. Arrows indicate two TMRE stained pericytes devoid of TMRE signal, indicating that they were able to transfer their mitochondria to the adjacent DRAQ-5 stained pericytes. (c) Similar dual-pericyte co-culture as in (b), clusters of TMRE-stained mitochondria can be seen in the numerous cytosolic processes interconnecting adjacent cells (e.g. white arrows). (d) TMRE-stained mitochondria at points of contact between two pericytes (white rectangle). (e) Amplification of the point of contact delimited by the white rectangle in (d). Red signal corresponds to TMRE stained mitochondria. Arrows indicate TMRE signal crossing the intercellular space. V: vesicles. (f) The same region as depicted in (e) following cytosolic staining with violet-BMQC. The boundary between both cells is indicated by dotted lines. V: The same vesicles indicated in (e) (marked for spatial reference).

received TMRE stained mitochondria. At 24 h of co-culture, TMRE was present in more than 90% of astrocytes, which now contained three times more TMRE than pericytes. Occludin depletion in pericytes strongly reduced the amount of mitochondria shared with astrocytes (Figure 6(a) and (b)). In contrast, pericytes scarcely shared mitochondria with endothelial cells or fibroblasts, and occludin depletion slightly increased this transfer (Supplemental Figure S5).

Transfer of glucose and mitochondria from brain microvessels to cultured astrocytes

To have a better understanding of the biological relevance of glucose and mitochondria transfer to astrocytes, we treated human astrocytes with endosulfan sulfate (ES, 100 mM, 4 h), which blocks lactate dehydrogenase, glucose-6-phosphate dehydrogenase, and impairs mitochondria electron transport. As the result, ~50% of astrocytes detached from the dish substrate, a large number showed enlarged bodies and loss of astrocytic processes, and only a few cells retained their normal morphology (Figure 6(c), middle image). However, the addition of isolated murine live microvessels, for 2 h, to ES-treated human astrocytes, attenuated those changes, largely preserving astrocytic morphology, and preventing cellular detachment (Figure 6(c), right image). Transfer of murine mitochondria and glucose was confirmed by staining the isolated murine microvessels with TMRE and allowing them to take up 2-NBDG before adding them to the petri dishes containing astrocytes. Two hours later,

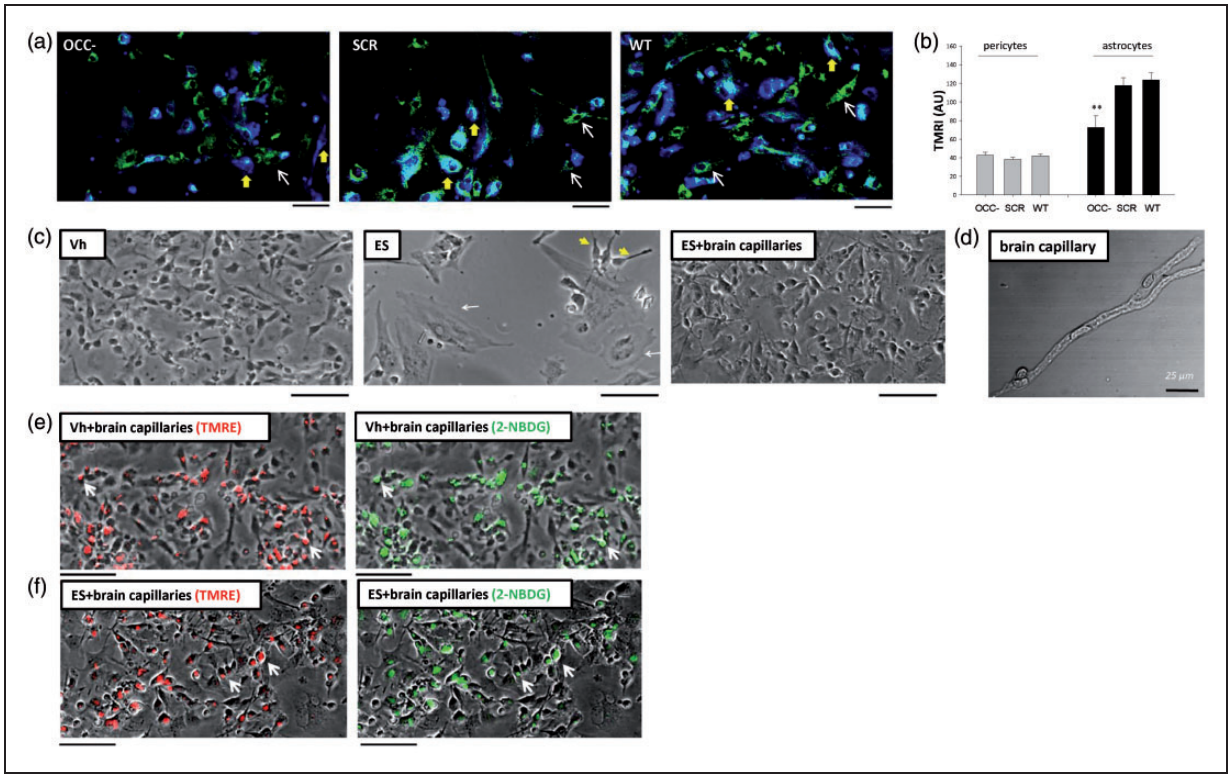

Figure 6. Pericytes share mitochondria with astrocytes in an occludin-mediated manner. (a) Live co-culture, 24 h post-plating, of astrocytes labeled with violet-BMQC (blue) and mitochondria-stained (TMRE in green) pericytes treated with anti-occludin siRNA (OCC−), negative-control siRNA (SCR), or non-treated (wild-type, WT). Thin white arrows exemplify TMRE-stained pericytes, while thick yellow arrows show pericyte mitochondria in the body of astrocytes (cyan signal). (b) Quantitation of TMRE intensities in astrocytes and pericytes in the same co-cultures shown in (a). Average ± SEM, $n = 25$ collected from three experiments, p vs. SCR. Only significant values are shown (c) Astrocytes treated with vehicle (Veh) or with endosulfan sulfate (ES, 4 h) to block their energetic metabolism. Middle image, surviving astrocytes exhibiting widened bodies and gross morphological alterations are exemplified by thin white arrows. Yellow arrowheads point to astrocytes that still retain their normal morphology. Right image: astrocytes treated with ES; however, isolated murine live brain capillaries (D shows a single brain capillary) were added to their growth medium 2 h post-treatment, and incubated for two additional hours. Note markedly improved astrocyte morphology. (e) Not-labeled human astrocytes cultured with murine live brain capillaries pre-labeled with TMRE (red) and 2-NBDG (green) for 2 h. TMRE and 2-NBDG transferred from microvessels to astrocytes (arrows) indicate transfer of mitochondria and glucose, respectively. (f) Similar TMRE and 2-NBDG transfer (arrows) in microvessel-rescued/ES-treated astrocytes after incubation with TMRE and 2-NBDG-labeled murine live brain capillaries.

TMRE and 2-NBDG were visible in the cellular bodies of normal (Figure 6(e)) and ES-treated astrocytes (Figure 6(f)). These observations show that occludin is not only able to regulate pericyte energetics and metabolic cascades, but also influences their capacity to share glucose and mitochondria with astrocytes.

Discussion

Among the critical functions of the BBB, glucose uptake and delivery from the blood to the neurons is of particular relevance as neurons depend on glucose to function.[36] The ability of the BBB to efficiently deliver glucose and directionally regulate the transport of water, nutrients, and metabolic waste is determinant of brain function.[7] Furthermore, metabolic crosstalk between cells of neurovascular unit is critical in controlling molecular transport across the BBB.[10,13] Our experiments show that pericyte glucose intake is four times higher than in endothelial cells, but similar to that of astrocytes, suggesting potential astrocyte/pericyte complementary roles in maintaining glucose homeostasis in the brain. Furthermore, astrocytes and pericytes express comparable amounts of the glucose transporters GLUT-1 and GLUT-4.

GLUT-1 is the main glucose transporter in the BBB.[8,37] It is crucial for neuronal metabolism, and defects on its function correlate with brain metabolic impairment, seizures, delayed development and acquired microcephaly in humans.[38] GLUT-1 is

expressed in response to NFκB, SP1, and AMPK activity,[39,40] and functions in an insulin-independent manner, ensuring that glucose transport across the BBB occurs in response to metabolic cues from the brain without glycemic constrains. The BBB also expresses GLUT-4 in an insulin-sensitive manner; however, it is mainly circumscribed to the hypothalamic ventromedial region,[41] which is highly sensitive to minor variations in glycemia. Similar to GLUT-1, GLUT-4 is also expressed in response to AMPK activation.[42]

While previous studies have shown that AMPK activity regulates cellular glucose uptake and transport across endothelial cells,[43,44] we observed that in pericytes, glucose uptake and GLUT-1/GLUT-4 depend not only on AMPK activity, but also on occludin levels. Similar to glucose transporters, AMPK expression and activation correlated with occludin levels, and increasing occludin expression caused elevation of GLUT1/GLUT4. Pharmacological inhibition of AMPK in occludin-overexpressing pericytes prevented occludin-mediated increase in GLUT-1 and GLUT-4 expression, indicating the need of AMPK activation for occludin to influence the expression of these glucose transporters. Similarly, occludin overexpression caused elevated glucose uptake in pericytes exposed to insulin, but inhibition of AMPK activity prevented this occludin-mediated phenomenon. The influence of occludin on AMPK activity was further evidenced by studying cellular ATP content. ATP levels in wild-type pericytes were incremented upon pharmacological activation of AMPK. Occludin depletion decreased ATP production; however, the administration of AICAR under occludin depletion conditions was unable to restore ATP levels, indicating that occludin was needed for AMPK activation. This correlates with previous reports showing that AMPK activation is NAD^+ sensitive,[32] and that the cellular NAD^+ content is proportional to occludin levels.[25] Treatment of pericytes with negative-control siRNA and dorsomorphin resulted in enhanced ATP production, which we attribute to off-target siRNA effects.

Our study also demonstrates that occludin colocalizes with lysosomes. This phenomenon has important relevance as lysosomes are subcellular hubs involved in secretion, plasma membrane repair, signaling, and energy metabolism.[45] Adequate lysosome function antagonizes HIV replication,[46] and we show that during the initial infection phase in pericytes, HIV not only reduces occludin expression but also decreased its localization to lysosomes. These effects correlate with lower AMPK activation levels and diminished glucose uptake. These findings expand our previous report on occludin function, where occludin is shown to be a NADH oxidase targeted by HIV in order to regulate SIRT-1 expression and activation, influencing NFκB activity, and enhancing viral replication.[25] Although these metabolic changes were closely associated with cellular occludin levels, it is still possible that they are secondary to other phenotypic alterations, like changes in proliferation occurring in parallel to occludin depletion. Indeed, TNFα treatment or HIV infection stimulated proliferation while causing occludin depletion. These findings are in agreement with literature reports showing that loss of occludin is a common denominator of cellular proliferation as occurs during metastasis of breast cancer[47,48] and hepatocellular carcinoma.[49] Similarly, loss of occludin causes reduced activation of apoptotic caspase-3.[50] In addition, increased proliferation of neural stem cells by a mechanism involving SIRT-1, CREB and Hes1 has been linked to low glucose availability,[51] which correlates with our present results, showing enhanced pericyte proliferation under low-glucose uptake conditions, and our previous findings demonstrating the functional dependency of SIRT-1 on occludin.[25] Furthermore, AMPK also plays a role regulating cell proliferation: its activation strongly inhibits proliferation in normal and tumor cells,[52] but in astrocytic tumors AMPK activation perpetuates cell growth.[53] Thus, occludin influence on glucose metabolism might represent a parallel process occurring during other metabolic changes of larger magnitude.

Our study demonstrated that pericytes readily shared glucose and mitochondria in co-cultures with astrocytes. In normal conditions, occludin appeared to mobilize mitochondria and increased pericyte glucose uptake. However, occludin depletion decreased pericyte capacity to transfer mitochondria, while enhancing their ability to deliver glucose and reducing their own glucose uptake. This translates into lower glucose influx paired with higher efflux. Although counterintuitive, this condition falls within tolerable functional limits as transmembranal glucose influx largely exceeds the rate at which even highly active cells (i.e. hepatocytes) can phosphorylate it.[54] Thus, it is possible that occludin loss may decrease glucose influx only to a level that approximates the capacity of pericytes to use it, and release any glucose excess if needed. This could ameliorate potentially imbalanced glucose-stimulated ROS production during injury. This process may play an important role in neuroinflammation, which associates with elevated TNFα levels that promote occludin downregulation.

Our findings also indicate that pericytes share glucose with astrocytes under energy deprivation conditions, which complements the recently demonstrated mitochondrial transfer between astrocytes and neurons providing energetic support to neurons during stroke.[55] We further observed that live brain microvessels promptly transfer mitochondria to endosulfan-exposed

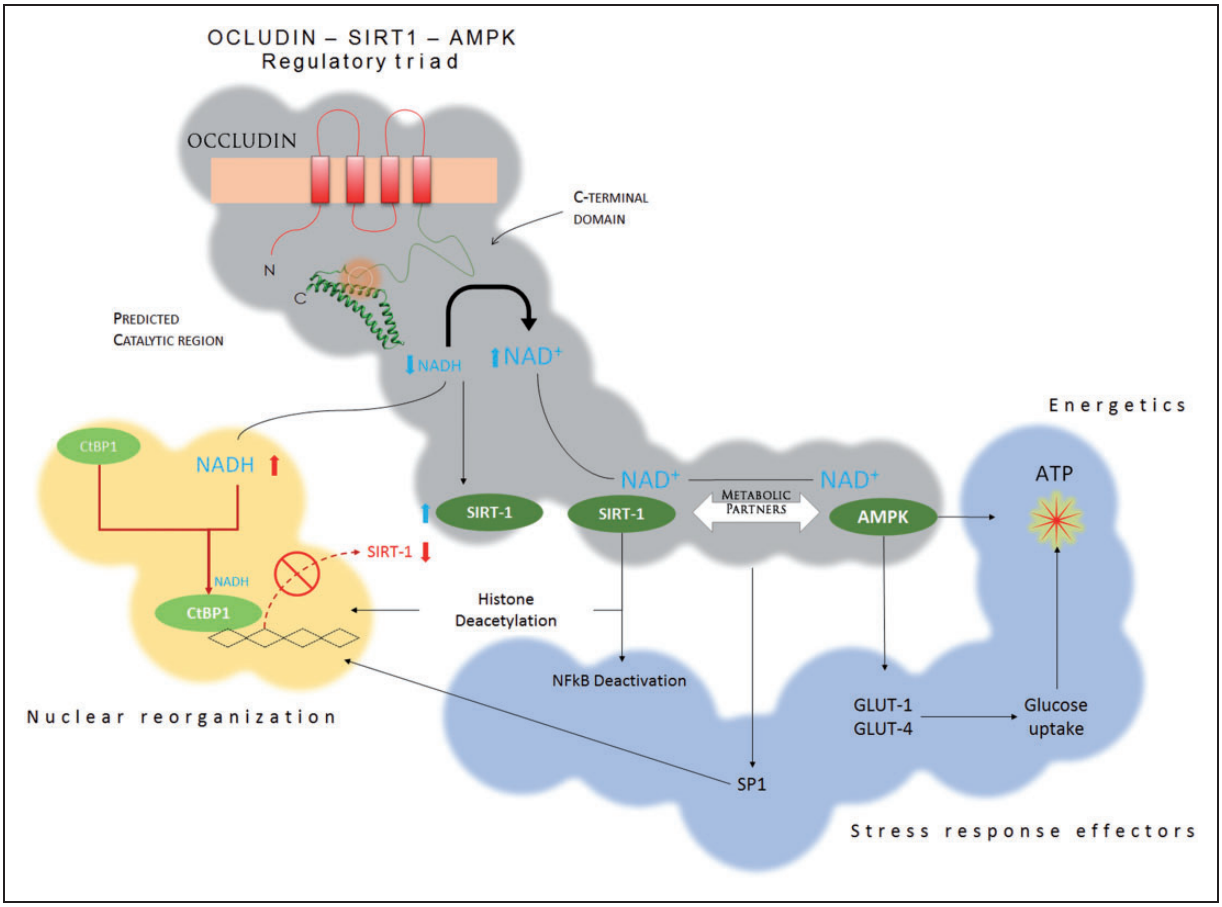

Figure 7. Occludin-AMPK-SIRT1 regulatory partnership. Stemming from its capacity as a NADH oxidase, occludin converts NADH into NAD+, reducing NADH availability, but increasing the pool of NAD+. This increases the expression of SIRT-1 by preventing CtBP1 from entering the cell nucleus, and enhances SIRT-1 activation by NAD+. Active SIRT-1 deacetylates histones and transcription factors, changing gene expression. However, SIRT-1 works in concert with AMPK, which is also sensitive to cellular NAD+, and active AMPK regulates critical metabolic pathways, including glucose uptake and ATP generation. By controlling the expression and activation of SIRT-1 and AMPK, occludin can influence critical metabolic pathways that integrate the cellular response to stress and cellular energetics.

astrocytes promoting their survival, and although this transfer could have originated from endothelial cells as well as pericytes, our results support the notion that mitochondrial transfer occurs readily between cells of the neurovascular unit in a manner that is sufficient to support potentially injured cells.

We also provide evidence that occludin is involved in expression and activation of NFκB and SP1, transcription factors that regulate expression of glucose transporters and mediate rapid response to metabolic stress, including inflammation. Occludin-mediated changes in the expression of AMPK, NFκB, SP1, GLUT-1 and GLUT-4 also correlated with spatial reorganization of the nucleosomal acetylated histone H2.A and linker histone H1. Altogether, this suggests that occludin plays a role in the epigenetic control of gene expression, and correlates with our previous work showing that occludin regulates expression of SIRT-1 by mediating nuclear translocation of CtBP1, and also promotes SIRT-1 activation by increasing NAD^+ production.[25] Downstream, SIRT-1 deacetylates NFκB, linking our previously described occludin-SIRT-1 interplay with our current observations demonstrating that acetylated levels of NFκB are consistently elevated upon occludin loss, but remain diminished in occludin-overexpressing cells.

Besides NFκB, the activities of several other transcription factors, such as SP1, p53, and p38MAPK, are regulated by acetylation.[56–58] They mediate the metabolic response to inflammation and stress, including cell growth, apoptosis, DNA repair, glucose metabolism, and production of inflammatory molecules such as TNFα and interleukins. It is thus possible that our findings only reflect a fraction of the spectrum of influence of occludin on cell metabolism. This idea is supported by our data showing that under the setting of

pericyte viral infection (HIV) and inflammation (TNFα), decreased occludin levels were associated with decreased glucose uptake and increased pericyte proliferation. We recently explored the relationship between occludin and metabolic alterations in pericytes following HIV infection and showed that occludin impairs viral proliferation.[25] This wide range of metabolic effects could be achieved if occludin was partnered with integrative metabolic players like AMPK and SIRT-1. Both influence gene expression, activation of transcription factors, glucose metabolism and cellular energetics,[28,59,60] and our current and previous[25] findings strongly indicate the existence of a metabolic regulatory triad: OCCLUDIN-AMPK-SIRT1 (Figure 7). This triple partnership is exemplified by our findings showing that pericytes become sensitive to insulin and enhance their glucose uptake in an AMPK-dependent manner when occludin levels are elevated, which is consistent with the involvement of SIRT1 and AMPK in regulation of insulin sensitivity.[61–63]

Although original reports described occludin as a membrane-bound protein localized in tight junctions,[64,65] it is now clear that many non-tight junction forming cells express occludin and that occludin is not always localized in the plasma membrane.[22,25] Nevertheless, the partnership of occludin with AMPK has also functional consequences for tight junctions in epithelial/endothelial cells. Occludin has been considered for long time a regulator of tight junction formation and function,[65–67] and our findings shed light on the precise mechanistic nature of this phenomenon as it has been shown that AMPK activity is needed for tight junction formation and polarization of epithelial/endothelial cells.[68] Furthermore, it is interesting that occludin, which can promote adhesiveness in non-tight junction forming cells,[69] can also influence sharing of glucose and mitochondria to different degrees, depending on cell-type, as it occurred between pericytes and astrocytes or pericytes and endothelial cells/fibroblasts. Moreover, it is still not clear whether membranal occludin in pericytes participates in forming junctional complexes with endothelial cells. The biological implications of these findings still need to be further explored.

Altogether our work shows how occludin is functionally associated with AMPK by localization at a metabolic crossroad that regulates critical aspects of cell metabolism, acquiring pathophysiological relevance in clinical conditions that alter the structure and function of the BBB. Indeed, occludin levels are sensitive to systemic inflammation and are lowered in stroke, HIV infection, and chronic peripheral pain.[25,66,70,71] Thus, our observations may provide the foundations to exercise novel therapeutic/preventive approaches to better preserve BBB and brain function in pathophysiological conditions.

Funding

The author(s) disclosed receipt of the following financial support for the research, authorship, and/or publication of this article: This work was supported by the National Institutes of Health (NIH), grants HL126559, DA039576, MH098891, MH63022, MH072567, and DA027569, as well as the Miami Center for AIDS Research funded by the NIH grant P30AI073961.

Declaration of conflicting interests

The author(s) declared no potential conflicts of interest with respect to the research, authorship, and/or publication of this article.

Authors' contributions

VC designed and conducted experiments, analyzed data, and wrote the manuscript; MS conducted experiments and analyzed data; JL contributed to experimental design and conducted experiments; JH, NS, and MV conducted experiments; and MT provided intellectual input, logistic and financial support.

Supplementary material

Supplementary material for this paper can be found at the journal website: http://journals.sagepub.com/home/jcb

References

1. Ballabh P, Braun A and Nedergaard M. The blood-brain barrier: an overview: structure, regulation, and clinical implications. *Neurobiol Dis* 2004; 16: 1–13.
2. Banerjee S and Bhat MA. Neuron-glial interactions in blood-brain barrier formation. *Annu Rev Neurosci* 2007; 30: 235–258.
3. Hervé J-C, Cereijido M, Contreras RG, et al. Tight junction and polarity interaction in the transporting epithelial phenotype. *Biochim Biophys Acta – Biomembr* 2008; 1778: 770–793.
4. Kinne RK. Endothelial and epithelial cells: general principles of selective vectorial transport. *Int J Microcirc Clin Exp* 1997; 17: 223–230.
5. O'Donnell ME. Blood-brain barrier Na transporters in ischemic stroke. *Adv Pharmacol* 2014; 71: 113–146.
6. Wang JD, Khafagy E-S, Khanafer K, et al. Organization of endothelial cells, pericytes, and astrocytes into a 3D microfluidic in vitro model of the blood-brain barrier. *Mol Pharm* 2016; 13: 895–906.
7. Hawkins BT and Davis TP. The blood-brain barrier/neurovascular unit in health and disease. *Pharmacol Rev* 2005; 57: 173–185.
8. Duelli R and Kuschinsky W. Brain glucose transporters: relationship to local energy demand. *News Physiol Sci* 2001; 16: 71–76.
9. Chuquet J, Quilichini P, Nimchinsky EA, et al. Predominant enhancement of glucose uptake in astrocytes versus neurons during activation of the somatosensory cortex. *J Neurosci* 2010; 30: 15298–15303.

10. Bonkowski D, Katyshev V, Balabanov RD, et al. The CNS microvascular pericyte: pericyte-astrocyte crosstalk in the regulation of tissue survival. *Fluids Barriers CNS* 2011; 8: 8.
11. Yao Y, Chen Z-L, Norris EH, et al. Astrocytic laminin regulates pericyte differentiation and maintains blood brain barrier integrity. *Nat Commun* 2014; 5: 3413.
12. Bergers G and Song S. The role of pericytes in blood-vessel formation and maintenance. *Neuro Oncol* 2005; 7: 452–464.
13. Armulik A, Abramsson A and Betsholtz C. Endothelial/pericyte interactions. *Circ Res* 2005; 97: 512–523.
14. Gerhardt H and Betsholtz C. Endothelial-pericyte interactions in angiogenesis. *Cell Tissue Res* 2003; 314: 15–23.
15. Prasad S and Cucullo L. Pericytes and astrocytes cross-talk: understanding perivascular synergism at the BBB. *FASEB J* 2013; 27: lb720.
16. Abbott NJ, Rönnbäck L and Hansson E. Astrocyte-endothelial interactions at the blood-brain barrier. *Nat Rev Neurosci* 2006; 7: 41–53.
17. Winkler EA, Sagare AP and Zlokovic B V. The pericyte: a forgotten cell type with important implications for Alzheimer's disease? *Brain Pathol* 2014; 24: 371–386.
18. Armulik A, Genové G, Mäe M, et al. Pericytes regulate the blood-brain barrier. *Nature* 2010; 468: 557–561.
19. Armulik A, Genové G and Betsholtz C. Pericytes: developmental, physiological, and pathological perspectives, problems, and promises. *Dev Cell* 2011; 21: 193–215.
20. Shimizu F, Sano Y, Maeda T, et al. Peripheral nerve pericytes originating from the blood-nerve barrier expresses tight junctional molecules and transporters as barrier-forming cells. *J Cell Physiol* 2008; 217: 388–399.
21. Zlokovic BV. The blood-brain barrier in health and chronic neurodegenerative disorders. *Neuron* 2008; 57: 178–201.
22. Bauer H, Stelzhammer W, Fuchs R, et al. Astrocytes and neurons express the tight junction-specific protein occludin in vitro. *Exp Cell Res* 1999; 250: 434–438.
23. Romanitan MO, Popescu BO, Winblad B, et al. Occludin is overexpressed in Alzheimer's disease and vascular dementia. *J Cell Mol Med* 2007; 11: 569–579.
24. Rescigno M, Rotta G, Valzasina B, et al. Dendritic cells shuttle microbes across gut epithelial monolayers. *Immunobiology* 2001; 204: 572–581.
25. Castro V, Bertrand L, Luethen M, et al. Occludin controls HIV transcription in brain pericytes via regulation of SIRT-1 activation. *FASEB J* 2016; 30: 1234–46.
26. Alexander JS, Dayton T, Davis C, et al. Activated T-lymphocytes express occludin, a component of tight junctions. *Inflammation* 1998; 22: 573–582.
27. Qiu L, Chen C, Ding G, et al. The effects of electromagnetic pulse on the protein levels of tight junction associated-proteins in the cerebral cortex, hippocampus, heart, lung, and testis of rats. *Biomed Environ Sci* 2011; 24: 438–444.
28. Ruderman NB, Xu XJ, Nelson L, et al. AMPK and SIRT1: a long-standing partnership? *Am J Physiol Endocrinol Metab* 2010; 298: E751–E760.
29. Kahn BB, Alquier T, Carling D, et al. AMP-activated protein kinase: ancient energy gauge provides clues to modern understanding of metabolism. *Cell Metab* 2005; 1: 15–25.
30. Russell RR, Bergeron R, Shulman GI, et al. Translocation of myocardial GLUT-4 and increased glucose uptake through activation of AMPK by AICAR. *Am J Physiol* 1999; 277: H643–H649.
31. Cantó C, Gerhart-Hines Z, Feige JN, et al. AMPK regulates energy expenditure by modulating NAD+ metabolism and SIRT1 activity. *Nature* 2009; 458: 1056–1060.
32. Rafaeloff-Phail R, Ding L, Conner L, et al. Biochemical regulation of mammalian AMP-activated protein kinase activity by NAD and NADH. *J Biol Chem* 2004; 279: 52934–52939.
33. Weksler B, Romero IA and Couraud P-O. The hCMEC/D3 cell line as a model of the human blood brain barrier. *Fluids Barriers CNS* 2013; 10: 16.
34. Howland SW, Gun SY, Claser C, et al. Measuring antigen presentation in mouse brain endothelial cells ex vivo and in vitro. *Nat Protoc* 2015; 10: 2016–2026.
35. Zhang C-S, Jiang B, Li M, et al. The lysosomal v-ATPase-Ragulator complex is a common activator for AMPK and mTORC1, acting as a switch between catabolism and anabolism. *Cell Metab* 2014; 20: 526–540.
36. Mergenthaler P, Lindauer U, Dienel GA, et al. Sugar for the brain: the role of glucose in physiological and pathological brain function. *Trends Neurosci* 2013; 36: 587–597.
37. Morgello S, Uson RR, Schwartz EJ, et al. The human blood-brain barrier glucose transporter (GLUT1) is a glucose transporter of gray matter astrocytes. *Glia* 1995; 14: 43–54.
38. Seidner G, Alvarez MG, Yeh JI, et al. GLUT-1 deficiency syndrome caused by haploinsufficiency of the blood-brain barrier hexose carrier. *Nat Genet* 1998; 18: 188–91.
39. Abbud W, Habinowski S, Zhang JZ, et al. Stimulation of AMP-activated protein kinase (AMPK) is associated with enhancement of Glut1-mediated glucose transport. *Arch Biochem Biophys* 2000; 380: 347–352.
40. Kao Y-S and Fong JC. Endothelin-1 induces glut1 transcription through enhanced interaction between Sp1 and NF-kappaB transcription factors. *Cell Signal* 2008; 20: 771–778.
41. Ngarmukos C, Baur EL and Kumagai AK. Co-localization of GLUT1 and GLUT4 in the blood-brain barrier of the rat ventromedial hypothalamus. *Brain Res* 2001; 900: 1–8.
42. McGee SL, van Denderen BJW, Howlett KF, et al. AMP-activated protein kinase regulates GLUT4 transcription by phosphorylating histone deacetylase 5. *Diabetes* 2008; 57: 860–867.
43. O'Neill HM. AMPK and exercise: glucose uptake and insulin sensitivity. *Diabetes Metab J* 2013; 37: 1–21.
44. Lee WL and Klip A. Shuttling glucose across brain microvessels, with a little help from GLUT1 and AMP kinase. Focus on 'AMP kinase regulation of sugar transport in brain capillary endothelial cells during acute metabolic stress'. *Am J Physiol Cell Physiol* 2012; 303: C803–C805.
45. Settembre C, Fraldi A, Medina DL, et al. Signals from the lysosome: a control centre for cellular clearance and

energy metabolism. *Nat Rev Mol Cell Biol* 2013; 14: 283–296.
46. Wei BL, Denton PW, O'Neill E, et al. Inhibition of lysosome and proteasome function enhances human immunodeficiency virus type 1 infection. *J Virol* 2005; 79: 5705–5712.
47. Martin TA, Mansel RE and Jiang WG. Loss of occludin leads to the progression of human breast cancer. *Int J Mol Med* 2010; 26: 723–734.
48. Martin TA, Jordan N, Davies EL, et al. Metastasis to bone in human cancer is associated with loss of occludin expression. *Anticancer Res* 2016; 36: 1287–1293.
49. Orbán E, Szabó E, Lotz G, et al. Different expression of occludin and ZO-1 in primary and metastatic liver tumors. *Pathol Oncol Res* 2008; 14: 299–306.
50. Beeman N, Webb PG and Baumgartner HK. Occludin is required for apoptosis when claudin-claudin interactions are disrupted. *Cell Death Dis* 2012; 3: e273.
51. Fusco S, Leone L, Barbati SA, et al. A CREB-Sirt1-Hes1 circuitry mediates neural stem cell response to glucose availability. *Cell Rep* 2016; 14: 1195–1205.
52. Motoshima H, Goldstein BJ, Igata M, et al. AMPK and cell proliferation–AMPK as a therapeutic target for atherosclerosis and cancer. *J Physiol* 2006; 574: 63–71.
53. Ríos M, Foretz M, Viollet B, et al. AMPK activation by oncogenesis is required to maintain cancer cell proliferation in astrocytic tumors. *Cancer Res* 2013; 73: 2628–38.
54. Fehr M, Takanaga H, Ehrhardt DW, et al. Evidence for high-capacity bidirectional glucose transport across the endoplasmic reticulum membrane by genetically encoded fluorescence resonance energy transfer nanosensors. *Mol Cell Biol* 2005; 25: 11102–11112.
55. Hayakawa K, Esposito E, Wang X, et al. Transfer of mitochondria from astrocytes to neurons after stroke. *Nature* 2016; 535: 551–555.
56. Waby JS, Chirakkal H, Yu C, et al. Sp1 acetylation is associated with loss of DNA binding at promoters associated with cell cycle arrest and cell death in a colon cell line. *Mol Cancer* 2010; 9: 275.
57. Tang Y, Zhao W, Chen Y, et al. Acetylation is indispensable for p53 activation. *Cell* 2008; 133: 612–626.
58. Pillai VB, Sundaresan NR, Samant SA, et al. Acetylation of a conserved lysine residue in the ATP binding pocket of p38 augments its kinase activity during hypertrophy of cardiomyocytes. *Mol Cell Biol* 2011; 31: 2349–2363.
59. Boily G, Seifert EL, Bevilacqua L, et al. SirT1 regulates energy metabolism and response to caloric restriction in mice. *PLoS One* 2008; 3: e1759.
60. Fullerton MD and Steinberg GR. SIRT1 takes a backseat to AMPK in the regulation of insulin sensitivity by resveratrol. *Diabetes* 2010; 59: 551–553.
61. Zachariah Tom R, Garcia-Roves PM, Sjögren RJO, et al. Effects of AMPK activation on insulin sensitivity and metabolism in leptin-deficient ob/ob mice. *Diabetes* 2014; 63: 1560–1571.
62. Sun C, Zhang F, Ge X, et al. SIRT1 improves insulin sensitivity under insulin-resistant conditions by repressing PTP1B. *Cell Metab* 2007; 6: 307–319.
63. Côté CD, Rasmussen BA, Duca FA, et al. Resveratrol activates duodenal Sirt1 to reverse insulin resistance in rats through a neuronal network. *Nat Med* 2015; 21: 498–505.
64. Furuse M, Hirase T, Itoh M, et al. Occludin: a novel integral membrane protein localizing at tight junctions. *J Cell Biol* 1993; 123: 1777–1788.
65. Cummins PM. Occludin: one protein, many forms. *Mol Cell Biol* 2012; 32: 242–50.
66. Blasig IE, Bellmann C, Cording J, et al. Occludin protein family: oxidative stress and reducing conditions. *Antioxid Redox Signal* 2011; 15: 1195–1219.
67. Feldman GJ, Mullin JM and Ryan MP. Occludin: structure, function and regulation. *Adv Drug Deliv Rev* 2005; 57: 883–917.
68. Zhang L, Li J, Young LH, et al. AMP-activated protein kinase regulates the assembly of epithelial tight junctions. *Proc Natl Acad Sci U S A* 2006; 103: 17272–17277.
69. Van Itallie and Anderson JM. Occludin confers adhesiveness when expressed in fibroblasts. *J Cell Sci* 1997; 110: 1113–1121.
70. Brooks TA, Hawkins BT, Huber JD, et al. Chronic inflammatory pain leads to increased blood-brain barrier permeability and tight junction protein alterations. *Am J Physiol Hear Circ Physiol* 2005; 289: H738–H743.
71. McCaffrey G, Seelbach MJ, Staatz WD, et al. Occludin oligomeric assembly at tight junctions of the blood-brain barrier is disrupted by peripheral inflammatory hyperalgesia. *J Neurochem* 2008; 106: 2395–2409.